Learning and Nonlinear Models - Journal of the Brazilian Society on Computational Intelligence (SBIC), Vol. 21, Iss. 1, pp. 60-76, 2023

A STATISTICAL SIGNAL PROCESSING APPROACH TO ISLANDING DETECTION

Robson Rosserrani de Lima, Augusto Santiago Cerqueira
Federal University of Juiz de Fora
robson.lima@engenharia.ufjf.br, augusto.santiago@ufjf.edu.br

Paulo Fernando Ribeiro
Federal University of Itajubá
pfribeiro@ieee.org

Danton Diego Ferreira
Federal University of Lavras, Automation Department
danton@ufla.br

Abstract – The integration of distributed generation (DG) sources in the electric energy systems may bring new problems that need attention, one of these problems is the occurrence of unintentional islanding. Islanding is a condition in which part of the distribution network is disconnected from the system, and consumer units are still powered by one or more DGs, which can cause damage to equipment and pose risks to the safety of technicians. This paper shows an islanding detection method (IDM) in Power Systems with DG based on statistical signal processing. We used a MathWorks Simulink model of a grid-connected 250 kW photovoltaic (PV) array to simulate the behavior of the three-phase voltage signal in the point of common coupling (PCC) under the nominal operation, islanding condition, and fault condition using different load compositions. Principal Component Analysis (PCA) was used to extract the transitory events from the voltage signals, and then we used second-, third-, and fourth-order cumulants to generate features and the best ones were selected using the Fisher's Discriminant Ratio (FDR). A Radial Basis Function Network (RBFN) makes the classification of the events. We found that, for this setup, we can achieve detection rates of 99% for both islanding condition detection and fault occurrence classification, no matter the power mismatch between the load and the DG.
Keywords – Islanding detection, distributed generation, principal component analysis, high order statistics, cumulants, radial basis function network, photovoltaic array, Fisher's discriminant ratio.

1 INTRODUCTION

The growing concern with sustainable electricity generation has encouraged the adoption of Distributed Generation (DG) systems [1]. In Brazil, generation by wind and photovoltaic (PV) sources currently corresponds to approximately 14% of the supervised power in the Brazilian energy matrix [2][1]. The Brazilian Association of Distributed Generation (ABGD) announced that in 2022, Brazil reached 9 GW of installed power in DG, mainly from photovoltaic sources (97.7%), and estimates that, even with the crisis generated by the coronavirus pandemic, by the end of the year it will be reached 15 GW of power [3][2].

The integration of these new sources through DG in the electric energy systems represents a change in the power generation paradigm in Brazil and the world [4], however, they bring with them the emergence of new problems that need attention. One of these problems is the occurrence of unintentional islanding.

Islanding is a condition in which part of the distribution network is disconnected from the system, and consumer units are still powered by one or more DG connected to them as depicted in Fig. 1. The islanding can be intentional or unintentional, and it is important to distinguish between controlled and uncontrolled island operations. The intentional island is a method to provide the reliability of supply when the service to local customers should be provided even without power grid connections. The unintentional island operation is a serious problem that should be avoided whenever possible. The main problems associated with an unintentional islanding condition are [5]:

- Threatens the security of technicians that perform the maintenance of the system;
- Loss of control of parameters such as voltage and frequency of the network by the concessionaire;
- Loss of coordination of protection devices against short circuits within the island;
- The islanded subsystem may have inadequate grounding conditions;

[1] Aviable on: ANEEL
[2] Aviable on: ABGD

- Energized islands can interfere with the restoration (manual or automatic) of the energy supply to consumers.

Although there are no specific tests for islanding operations in Brazil, it is possible to rely on some international standards such as IEEE Std. 1547–2003 [6], which sets the standards for voltage and current at the point of common coupling (PCC) in addition to specifying that the DG system must be disconnected within 2 seconds when islanding occurs.

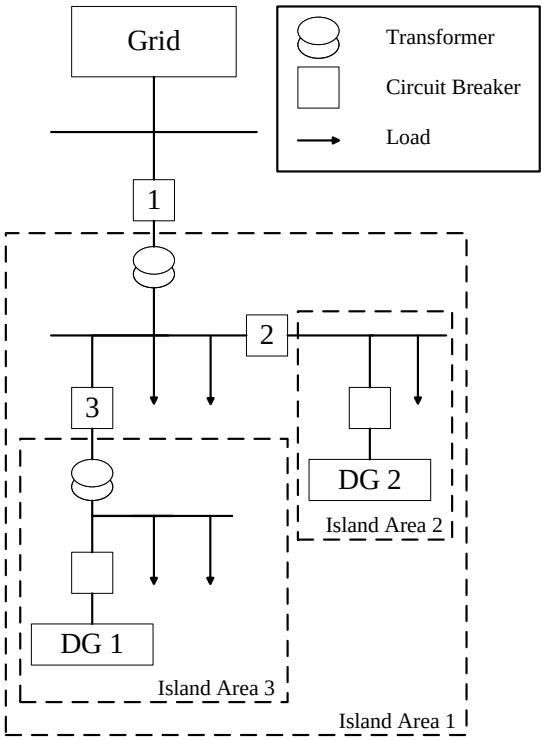

Figure 1: Simple islanding concept. Island area 1, 2 and 3 are formed by opening of circuit breaker 1, 2 and 3 respectively. Source: adapted from [7]

Several islanding detection methods (IDM) have been proposed over the years, which can be broadly classified into classic and modern methods. As depicted in Fig. 2, the former can also be sub-classified as passive, active, hybrid, or remote, while the latter is based on signal processing and classification [7]. The classic passive methods, being the Rate of Change of Frequency (ROCOF) [8, 9] one of the most common, are based on the measurement of certain parameters, like the frequency, in the PCC or DG terminals and compared with a predetermined threshold to detect islanding. Although they have low cost and fast detection times, these methods suffer from nuisance tripping and large non-detection zones (NDZ), *i.e.*, the operation region of an IDM in which islanding cannot be determined [7]. With smaller NDZ, but with the inconvenience of causing degradation of the grid power quality, the active methods are based on sending a disturbing signal to some network parameter and monitoring the effects of this signal on the PCC. Some common IDM in this category are the Slip Mode Frequency Shift (SMS) [10–12], Active Frequency Drift (AFD) [13–15], Sandia Frequency Shift (SFS) [12, 16, 17], and Sandia Voltage Shift (SVS) [12, 18]. The hybrid approaches in the classic branch of the IDM try to combine both passive and active techniques to obtain the advantages of these methods. Normally, the active techniques are applied only after a passive detection of islanding, diminishing the effect on power quality and achieving low NDZ [7]. Positive feedback (PF) and voltage unbalance (VU) [19], Voltage and reactive power shift [20], Hybrid SFS and Q-f [21], Voltage and real power shift (RPS) [22] are some of the hybrid techniques. Finally, the remote methods, such as the transfer trip scheme [23, 24] and power line carrier communication (PLCC) [25, 26], are based on the communication between the utility grid and the DGs. They have the advantage of a zero NDZ, but for small or single DG installation, the cost of implementation becomes very high [7].

Recently, using classic methods as starting points - mainly passive ones - more modern methods based on signal processing tools and classifiers have brought improvements to the performance of IDMs, achieving very low ZND, no impact on power quality, and low implementation costs. The signal processing methods usually extract features of the signals obtained in the PCC to perform islanding detection. Some of the most used techniques in these categories are the Wavelet Transform (WT) and its variants [27–31], Stockwell Transform (ST) [32, 33], Hilbert Huyang Transform (HHT) [34], Time-time Transform (TTT) [32, 35], mathematical morphology (MM) [32], and Principal Component Analysis (PCA) [36–39]. When the feature space provided by the signal processing methods does not provide a clear signature of the islanding condition, setting a threshold for the detection has been proved to be difficult. In these cases, classifier methods can be used to process these features and define a highly sensitive and accurate threshold. IDMs based on artificial neural network (ANN) [40–46], fuzzy logic (FL) [47, 48], artificial neural fuzzy inference system (ANFIS) [49–51], decision tree (DT) [40, 52, 53], and support vector machines (SVM) [32, 44] are prevalent nowadays and can achieve negligible to zero NDZ.

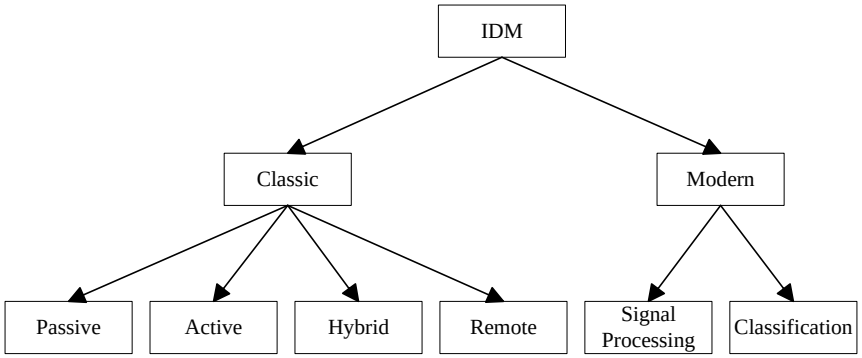

Figure 2: IDM classifications.

In this paper, a passive signal processing IDM is proposed for islanding detection using statistical signal processing techniques like principal component analysis (PCA) and high order statistics (HOS). It uses PCA as a way to extract a one-dimensional representation of the transitory events from the PCC three-phased voltage signal, then the cumulants are used as features to characterize the events between nominal operation, faults events, and islanding operation. The final classification is performed by a Radial Basis Function Network (RBFN). This type of architecture is easy to be designed and presents quick training, usually performed by a two-step algorithm, and with minimal input parameter (only the error goal and spreading of the radial basis functions must be provided [54]). Other ANN architectures, such as the Multi-layer Perceptron (MLP), can present good results for ID, as shown in [46], but it is conditioned to the choice of architecture, activation functions, and training algorithms, adding an extra layer of complexity for its development. Another method that requires a few input parameters is SVM. However, as shown in [43], which compared SVM, DT, and Probabilistic Neural Networks (PNN), there are indications that SVM performs worse than DT and PNN for islanding detection.

The main contributions of this article reside in the way that statistical signal processing techniques are combined to design an accurate and low complex islanding detection method. First, to the best of our knowledge, this is the first time that PCA is used in the three-phase voltage signal as a way of characterizing transient events for this type of phenomenon. Secondly, this is also the first time that HOS in the form of cumulants is used, in this context, as a feature extractor for the characterization of islanding events. In addition to proving to be an effective IDM, this new methodology opens up a new research space for the islanding problem.

The rest of the text is organized as follows. Section 2 presents the model used to simulate the dataset. In Section 3, the simulation tests and conditions are described. The proposed method is presented in Section 4. The simulation results are given in Section 5. Finally, the paper is concluded in Section 6.

2 GD MODELING

To generate the dataset used for the evaluation of the proposed method, a PV array of 250kW connected to the utility grid via a three-phase converter was used. The model was developed in Simulink [55] [3], and is depicted in Fig. 3. Each component is detailed as follows:

A. PV Array

The PV array contains 91 parallel strings, each containing 7 SunPower SPR-415E-WHT-D modules connected in series. It delivers a maximum power of 250kW at 1kW/m^2 sun irradiance and cell temperature of 45°C.

B. Three-Phase DC/AC Converter

The converter model is constructed using a PWM-controlled 3-level IGBT bridge. The harmonics generated by the IGBT bridge are filtered using the inverter choke and a small harmonics filter. The system is connected to the utility distribution grid with a 250V/25kV three-phase transformer of 250kVA [55].

C. Inverter Control

This control system can be divided into five subsystems [55]:

1) Maximum Power Point Tracking (MPPT) Controller: an MPPT controller based on the 'Perturb and Observe' technique [56] is used. This MPPT system determines the V_{DC} reference signal for the inverter V_{DC} regulator. It changes the reference signal to set the DC voltage which extracts the maximum power from the PV array.
2) V_{DC} Regulator: this subsystem defines the active current (I_d) reference for the current regulator.
3) Current Regulator: based on the I_d and I_q (reactive current), this regulator defines the voltage references for the inverter. Here, the I_q reference is set to zero.

[3] Aviable on: https://www.mathworks.com/help/physmod/sps/ug/250-kw-grid-connected-pv-array.html

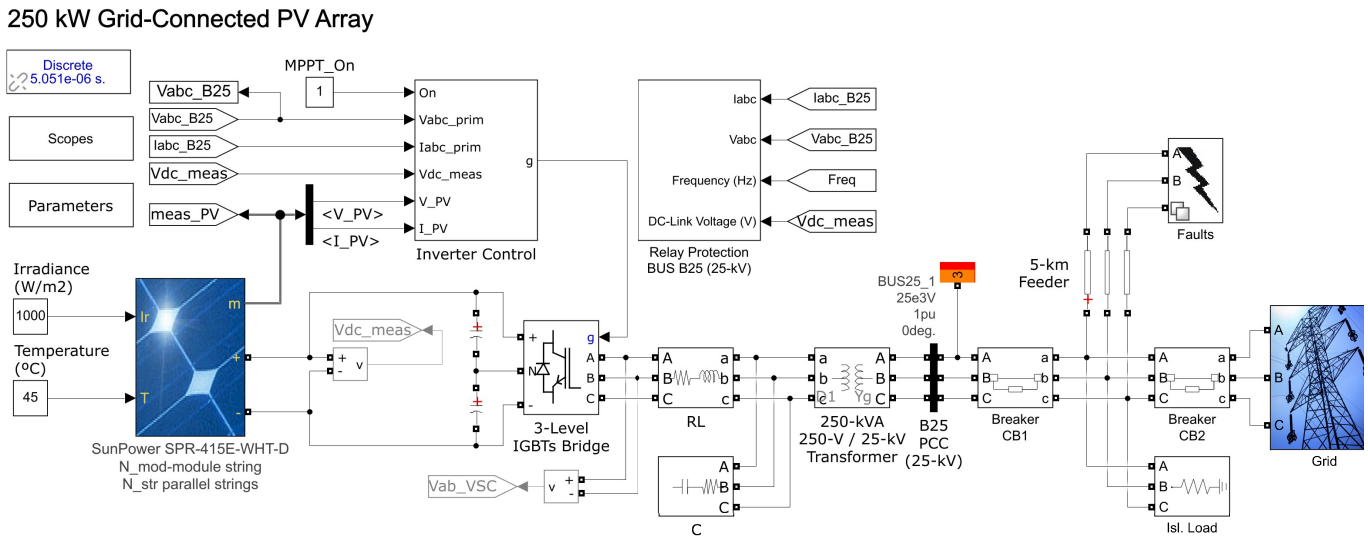

Figure 3: Detailed model of an 250kW grid-connected PV array.

4) Phased Locked Loop (PLL): a PLL [57] is used to synchronize the control system and provides a measure for the frequency of the system.
5) Pulse Width Modulation (PWM) Generator: it generates the firing signals to the IGBT bridge based on the reference voltages. It uses a carrier with a frequency of 1980 Hz.

D. Utility Grid

The utility grid was simulated as a 120kV transmission system. It contains a 120kV/25kV three-phase transformer of 47MVA, a grounding transformer, an 14km, and an 8km feeder, and two loads, one of 30MW and 2MVAr and one of 2MW.

E. Islanding and Three-Phase Fault

The island can be formed by opening the circuit-breaker CB2 (Fig. 3) between the utility grid and the local load, causing the latter to be powered only by the PV array. A three-phase fault component was also added to simulate different situations that can be, in some cases, confused with islanding.

F. IDM Relays

A series of common passive IDM schemes were implemented to be compared with the proposed method. Their implementation is shown in Figs. 4–6.

The Over/Under Voltage Protection (OVP/UVP) relays [7], shown in Fig. 4, and Over/Under Frequency protection (OFP/UFP) relays [7], shown in Fig. 5, are based in the same principle, they compare their respective parameters with a preset threshold. The active and reactive power imbalances at the PCC can be expressed as in Eqs. (1)–(2). If $\Delta P \neq 0$, the voltage amplitude will change according to Eq. (3) and the OVP/UVP detects islanding if it exceeds a limit. If $\Delta Q \neq 0$, the frequency of the system will change according to Eq. (4) and the OFP/UFP will trip if it crosses the thresholds. These thresholds are determined based on IEEE Std. 1547–2003 [6], and the frequency, in this simulation, is estimated by the PLL module.

$$\Delta P = P_{LOAD} - P_{DG}, \tag{1}$$

$$\Delta Q = Q_{LOAD} - Q_{DG}, \tag{2}$$

$$V' = \sqrt{P_{DG}/P_{LOAD}} \times V, \tag{3}$$

$$Q' = Q_{DG} = [(1/\omega' \times L) - \omega' \times C] \times V', \tag{4}$$

where ΔP and ΔQ are the active and reactive power mismatches, P_{DG} and Q_{DG} are the DG active and reactive powers, P_{LOAD} and Q_{LOAD} are the load active and reactive powers, V' is the PCC voltage after islanding, V is the rated voltage, ω' is the PCC angular frequency after islanding, L is the load inductance (H), and C is the load capacitance (F).

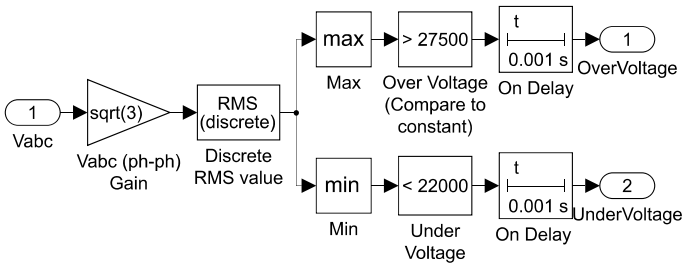

Figure 4: Simulink model of OVP/UVP.

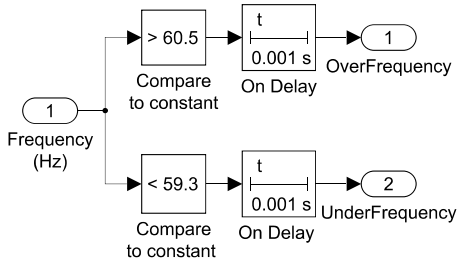

Figure 5: Simulink model of OFP/UFP.

The ROCOF relay [8], which implementation is depicted in Fig. 6, is based on the changes caused in the system frequency on grid supply disconnection. The ROCOF is measured over a few cycles and can be expressed as in Eq. (5). This implementation monitors the PV inverter frequency (estimated on PLL) to calculate the ROCOF. The threshold was defined as 12Hz/s as suggested in [58].

$$df/dt = (\Delta P \times f)/(2 \times H \times G) \tag{5}$$

where f is the main grid frequency, H is the moment of inertia of DG, and G is the rated generation capacity of DG.

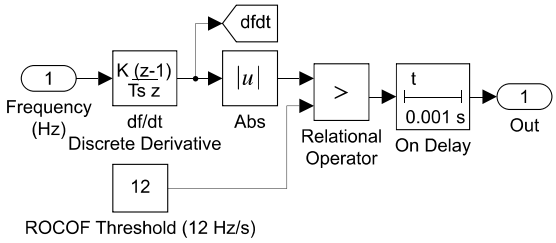

Figure 6: Simulink model of ROCOF protection.

3 SIMULATION FRAMEWORK

This section presents the structure of the simulation performed to generate the database used to test and validate the proposed method. The power requirements for the studied islanded load are defined, as well as how the islanding and fault condition occurred. The types of studied signals, their duration, and sampling frequency are also presented here.

3.1 Local Load Power Requirements

One way to determine the NDZ is using the power mismatch space (PMS). Under an islanding condition, the frequency and voltage in the PCC are determined by the active and reactive power imbalances between the DG production and the load consumption [7]. The limits of the NDZ in which an IDM fails [59] can be given by

$$(V/V_{max})^2 - 1 \leq (\Delta P/P_{DG}) \leq (V/V_{min})^2 - 1, \tag{6}$$

and

$$Q_f(1 - (f/f_{min})^2) \leq (\Delta Q/P_{DG}) \leq Q_f(1 - (f/f_{max})^2), \tag{7}$$

where V is the nominal voltage, P_{DG} is the DG active power, ΔP and ΔQ are the active and reactive power mismatches, respectively, Q_f is the quality factor, and f is the fundamental grid frequency. The IEEE Std. 1547–2003 set the under and over limits for the voltage and frequency as $V_{max} = 110\%$, $V_{min} = 88\%$, and $f_{max} = 60.5$Hz, $f_{min} = 59.3$Hz, respectively, with a $Q_f = 1$. Plugging these values in Eqs. (6) and (7) we obtain the permitted NDZ for this standard:

$$-17.36\% \leq (\Delta P/P_{DG}) \leq 29.13\% \tag{8}$$

$$-2.37\% \leq (\Delta Q/P_{DG}) \leq 1.65\% \tag{9}$$

Using the results of Eq. (8)–(9), the characteristics of the local islanded load were set to match eight points in the NDZ frontier plus its central point. The actual values for the active and reactive power of the load, considering $P_{DG} = 250$kW, are presented in Table 1.

Table 1: Local Load Active and Reactive Power Requirements

NDZ Points	**P (kW)**	**Q (kVAr)**
1 – min. ΔP and min. ΔQ	206.6	-5.9
2 – zero ΔP and min. ΔQ	250.0	-5.9
3 – max. ΔP and min. ΔQ	322.8	-5.9
4 – min. ΔP and zero ΔQ	206.6	0
5 – zero ΔP and zero ΔQ	250.0	0
6 – max. ΔP and zero ΔQ	322.8	0
7 – min. ΔP and max. ΔQ	206.6	4.1
8 – zero ΔP and max. ΔQ	250.0	4.1
9 – min. ΔP and max. ΔQ	322.8	4.1

The nine power profiles for the local load described in Table 1 were used to design the proposed method, being 5 considered the worst-case scenario, where there are no mismatches between the power delivered by the PV array and the required by the load [7]. Additionally, 100 other random points within the NDZ boundary were chosen to compose the database, resulting in a total of 109 power profiles.

3.2 Islanding and Fault Simulations

The model was simulated for each 109 loads power profiles under three distinct conditions: nominal, islanding, and fault. In the nominal operation, neither fault nor islanding occurred and the load was supplied both by the PV array and the utility grid. For the islanding operation, the circuit-breaker CB2 was opened for 100ms, during that time the load was supplied only by the PV array. Finally, for the fault condition, 11 different types were tested, say: A-G, B-G, C-G, A-B, B-C, C-A, A-B-G, B-C-G, C-A-G, A-B-C, and A-B-C-G, where A, B, and C correspond to the phases and G to the ground. These events occurred 5km from the PCC and also had a duration of 100ms.

Each combination load/condition was simulated for 0.7s using a sampling frequency of 198kHz. The tripping times for the islanding and fault conditions were fixed at 0.4s. The signals used for the analysis were the three-phase voltage at PCC. Finally, the first 0.2s of the signals are removed to exclude the period before the system stabilized, resulting in signals lasting 0.5s.

3.3 Database

The database can be divided into two sets, one used for method design and the other for its validation.

The design set is made up of all load/condition combinations described above, so each load described in Table 1 was simulated for nominal operation, for islanding, and the 11 fault types, so it contains 117 three-phase voltage signals (9 nominal signals, 9 islandings, and 99 faults) of 0.5s duration, representing the boundaries and the central point of the IEEE Std. 1547–2003 NDZ. As we don't distinguish between the fault types, this class is overrepresented in this set, so are expected some misclassifications.

The validation set consists of the load/condition combinations of the 100 random profiles described at the end of section 3.1. Here, each profile was tested for the nominal and islanding operation as described in section 3.2, but for fault condition, the event type was also random. So, the final validation database was composed of 300 three-phase voltage signals (100 for each condition) of 0.5s duration. Additionally, to investigate the sensitivity of the method to a noisy environment, white Gaussian noise with SNR ranging from 50 to 80 dB was added to the database.

4 PROPOSED METHOD

The proposed method has two phases, one for design and one for operation. In the design phase, the techniques are applied and their results are evaluated, leading to the choice of the most appropriate transformations and parameters for the studied scenario. These results allow the simplification of the operation phase, avoiding excessive or unnecessary calculations. Below we present the method in more detail.

4.1 Design Phase

Figure 7 shows a summary of the design phase. The three-phase voltage signal is measured at the PCC (see Fig. 3), then a representation of the transient events is extracted by performing a Principal Component Analysis (PCA). From these transients, features based on second-, third-, and fourth-order cumulants are extracted, and the best ones are selected using the Fisher's Discriminant Ratio (FDR) and used as input features in a Radial Basis Neural Network (RBNN) that performs the classification of signals into nominal, islanding or fault. Each technique employed and its main formulation are presented as follows.

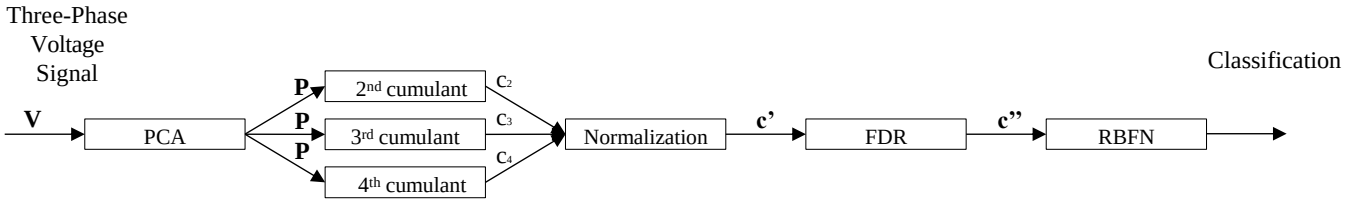

Figure 7: Simplified flowchart of the design phase.

4.1.1 Signal transformation with PCA

PCA is an orthogonal linear transformation used to convert a set of observations of possibly correlated variables into a set of uncorrelated linear values called Principal Components. Axes are rotated in such a way that the first component (the first coordinate in this new feature space) coincides with the direction of the greatest variance in the data, and the second component coincides with the direction of the second greatest variance, and so on. This method can be used to extract the most important information from a dataset [60]. Eq. (10) shows the PCA model, the goal is to find a rotation matrix $\mathbf{R}$ that maps the data set $\mathbf{V}$ into $\mathbf{P}$. Mathematically, this can be done using eigen decomposition of positive semi-definite matrices and singular vector decomposition (SVD) of rectangular matrices.

$$\mathbf{P} = \mathbf{RV} \tag{10}$$

In (10), $\mathbf{V}$ is a $k \times 3$ matrix corresponding to the three-phase voltage signal measured in the PCC, where k is the number of data points and each of the 3 phases is considered a variable, $\mathbf{R}$ is a 3×3 rotation matrix and $\mathbf{P}$ is a $k \times 3$ matrix with the principal components. Once $\mathbf{R}$ is found, a particular principal component can be extracted by selecting the appropriate column of $\mathbf{R}$. Used in this way, PCA can separate the sinusoidal components of the voltage signal (which is the most redundant information) from the events of interest. With this, the transient part of the signal is revealed in one or two principal components, and this part is used to distinguish the islanding events from the fault events and nominal conditions.

4.1.2 Feature extraction with HOS

To extract relevant features for Islanding detection, High Order Statistics (HOS) are used in terms of second-, third-, and fourth-order cumulants. In [61], it is demonstrated that cumulants are appropriate for use in electrical signals and capable of bringing a good characterization of electrical disturbances. In this paper, we use the stochastic approximations for the cumulants according to [61]. The formulation for the second-, third-, and fourth-order cumulants are shown in Eqs. (11)–(13), respectively.

$$\hat{c}_{2,p}[i] := \frac{1}{N} \sum_{n=0}^{N-1} p[n]p[\mathrm{mod}[n+1, N]] \tag{11}$$

$$\hat{c}_{3,p}[i] := \frac{1}{N} \sum_{n=0}^{N-1} p[n]p^2[\mathrm{mod}[n+1, N]] \tag{12}$$

$$\hat{c}_{4,p}[i] := \frac{1}{N} \sum_{n=0}^{N-1} p[n]p^3[\mathrm{mod}[n+1, N]] - \frac{1}{N^2} \sum_{n=0}^{N-1} p[n]p[\mathrm{mod}[n+1, N]] \sum_{n=0}^{N-1} p^2[n] \tag{13}$$

where $p[n]$ is the n-th element of the selected principal component; i is the i-th lag, with $i = 1, ..., N$; N is the length of the signal; and $\mathrm{mod}[n+1, N]$ is the entire remainder of the division of $n+1$ by N.

4.1.3 Data normalization

To avoid that features with large values may have a larger influence in the cost function of the classifier than features with small values, each cumulant was normalized into the range $[-1, 1]$ using the min-max feature scaling, as in Eq. (14).

$$\mathbf{c}' = 2 \cdot \frac{\mathbf{c} - \min(\mathbf{c})}{\max(\mathbf{c}) - \min(\mathbf{c})} - 1 \tag{14}$$

where $\mathbf{c}$ is one of the cumulant feature vectors, $\min(\mathbf{c})$ and $\max(\mathbf{c})$ are the minimum and maximum values of that vector, respectively, and $\mathbf{c}'$ is the scaled feature vector.

4.1.4 Feature selection

To find the best cumulants, we use the Fisher's Discriminant Ratio (FDR) [62]. The FDR assigns a score to each feature based on the ability to linearly separate the data in that dimension. Here, we consider three classes: nominal, islanding, and fault, so the FDR multi-class approach is used as formulated in Eq. (15).

$$FDR = \sum_{i}^{M} \sum_{j \neq i}^{M} \frac{(\mu_i - \mu_j)^2}{(\sigma_i^2 + \sigma_j^2)} \tag{15}$$

where $M = 3$ is the number of classes, the subscripts i, j refer to the mean (μ) and variance (σ^2) corresponding to the feature under investigation for the classes ω_i e ω_j, respectively. The greater the value of FDR in Eq. (15), greater is the relevance of the corresponding feature to distinguish the classes.

4.1.5 Classifier design

Finally, the selected cumulants are presented to a Radial Basis Function Network (RBFN) [54]. The radial basis (RB) neuron model is presented in Eq. (16).

$$a_{1,i} = e^{-(\|\mathbf{w}_{1,i} - \mathbf{c}\| \cdot b_{1,i})^2} \tag{16}$$

where $\mathbf{c}$ is an input vector, here it is the vector with the cumulants selected by Eq. (15); $\mathbf{w}_{1,i}$ is the weight vector; $b_{1,i}$ is the bias value; and the operator $\|\cdot\|$ denotes the Euclidean distance. These neurons form the first layer of the RBFN, so the subscripts '$1, i$' correspond to the i-th neuron of layer 1. The second layer is formed by linear neurons, whose model can be seen in Eq. (17).

$$a_{2,j} = \mathbf{w}_{2,j} \cdot \mathbf{a}_1 + b_{2,j} \tag{17}$$

where $\mathbf{w}_{2,j}$ is the weight vector; $\mathbf{a}_1$ is the vector containing all the outputs of the first layer; and $b_{2,j}$ is the bias value. Similar to the previous layer, the subscripts '$2, j$' correspond to the j-th neuron of layer 2.

Usually, this type of neural network is trained with a two-step algorithm: first, we define the number of RB neurons to be equal to the number of examples in the dataset and we set the weights of neurons equal to the values of the examples ($\mathbf{w}_1 = \mathbf{C}$), where $\mathbf{C}$ can be understood as a matrix representing all dataset; secondly, the weights of the linear layer are defined according to some objective function, commonly the minimization of the mean square error (MSE). As this approach can lead to architectures with many neurons, especially when compared to feed-forward networks, in this paper we use an iterative approach to network construction. First, the network has no RB neurons, it's then simulated, the input vector that generates the greatest error is identified, a new RB neuron is added with weights equal to that vector, and the weights of the linear layer are redesigned to minimize the MSE. These steps are repeated until an error goal is achieved. The bias of the first layer can be understood as a way to control the sensitivity $[s]$ or the width of the radial basis functions, setting $b_{1,i} = 0.8326/s$, the radial basis functions cross 0.5 at weighted inputs of $\pm s$, so if $\|\mathbf{w}_{1,i} - \mathbf{c}\| = s$, then $a_{1,i} = 0.5$.

4.2 Operational phase

Once the design phase is completed, the operational aspect of the method can be done as per Figure 8.

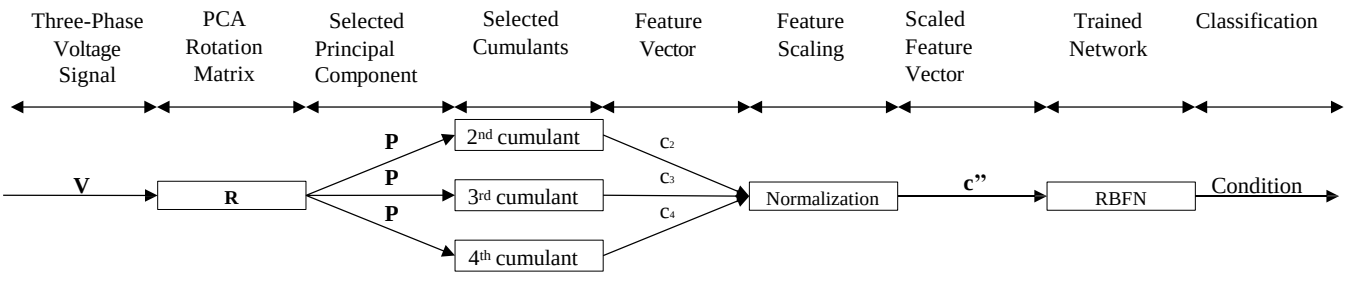

Figure 8: Flowchart of the operation phase.

As can be observed, once the rotation matrix $\mathbf{R}$ is found, the principal components can be estimated just by multiplying the input vector (three-phase voltage) by the corresponding column of the matrix. To extract the selected cumulants, it is not necessary to calculate all the lags, since they were already selected in the design phase using the FDR, being then enough to make the corresponding calculation directly from the principal component. For the data normalization, it is used the minimum and maximum values used in Eq. (14) to ensure that the feature scaling was respected. Once these steps are done, the scaled feature vector is presented to the trained RBFN to perform the classification.

To get an idea of the computational complexity of the proposed method in the operational phase, the number of mathematical operations required in each stage in terms of sum, multiplications, and nonlinear functions may be used. Table 2 summarizes the number of mathematical operations required by the proposed method in terms of the length (N) of the processing signal window and the number of neurons in the first (N_{n1}) and second (N_{n2}) layers of the RBFN.

Table 2: Number of mathematical operations required by the proposed method in the operational phase

Operation	**PCA**	**Cumulants**			**Normalization**	**RBFN**
		2^{nd} Order	**3^{rd} Order**	**4^{th} Order**		
Sums	$2N$	$N-1$	$N-1$	$3N-2$	$N+2$	$N_{n1}N_{n2}-N_{n2}+2N_{n1}+1$
Multiplications	$3N$	$N+1$	$2N+1$	$5(N+1)$	$N+1$	$N_{n1}(N_{n2}+3)+6$
Square Root	0	0	0	0	0	N_{n1}
Exponential	0	0	0	0	0	N_{n1}

5 SIMULATED RESULTS

In this section, the simulation results are presented. Unless otherwise specified, all images and examples refer to load profile 5 (see Table 1), where there is no power mismatch between load and DG. To faults, the examples shown are line-line faults between A and B.

The following sections present the results of the design and operation phases of the proposed method.

5.1 Design Results

Fig. 9 depicts the details of a three-phase voltage signal example for each condition analyzed. It can be observed that the islanding and nominal condition don't present any visible difference.

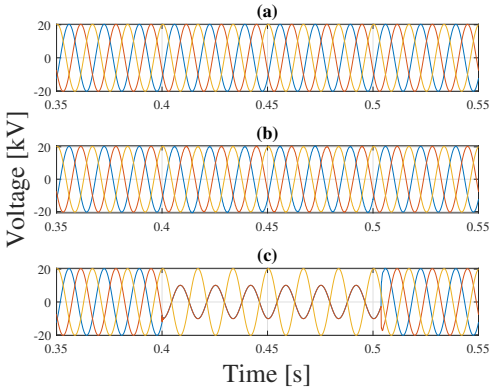

Figure 9: Detail between $t = 0.35s$ and $t = 0.55s$ of the three-phase voltage signal for (a) nominal condition, (b) islanding condition, and (c) line-line fault considering a local load with power requirements of $250kW$ ($\Delta P = \Delta Q = 0$).

PCA was applied to obtain a representation of the signal's transients, 'filtering' the redundant sinusoidal components. To achieve this, the nine design nominal signals were concatenated along the time axis, and used to perform the PCA, obtaining the following rotation matrix:

$$\mathbf{R} = \begin{bmatrix} -0.4700 & -0.6677 & 0.5774 \\ -0.3432 & 0.7409 & 0.5774 \\ 0.8132 & -0.0732 & 0.5774 \end{bmatrix} \tag{18}$$

In Fig. 10 we can see the principal components estimated using $\mathbf{R}$. It can be observed that the sinusoidal components are mainly represented by the first and second principal components, while the transients are more represented by the third component.

The sinusoidal part of the signal was concentrated in the first and second principal components for nominal operation (Fig. 10a) and the third component contains only a soft noise. The same behavior can be observed in the principal components for

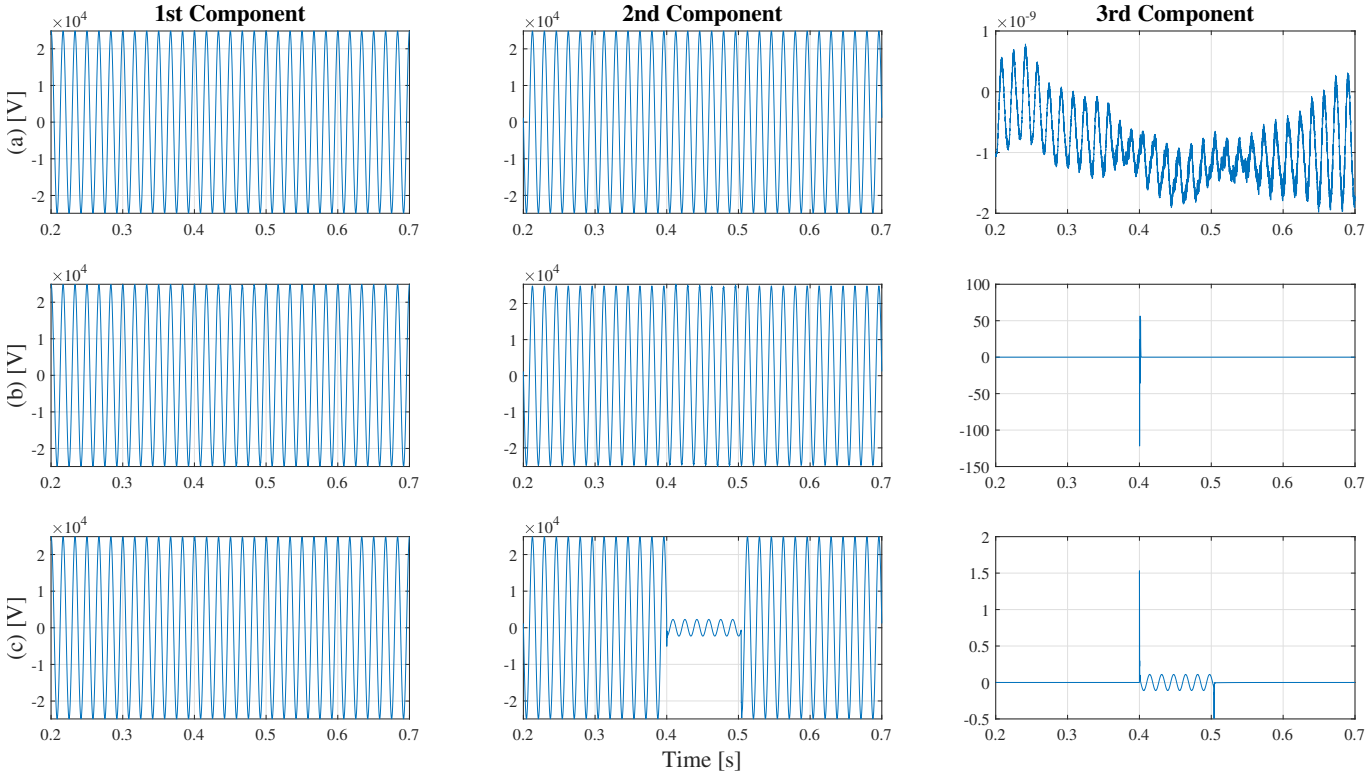

Figure 10: An example of the PCA results for (a) nominal, (b) islanding, and (c) A-B fault. It can be observed that each condition presents a distinct pattern.

the islanding operation (Fig. 10b), with the third component showing a spike at the beginning of the islanding. Finally, for the A-B fault, during their occurrence between $t = 0.4$ e $t = 0.5$, the second component presents a drop in their amplitude, and the third component shows a spike at the beginning and end of the disturbance with a sinusoidal behavior between them. The amplitude of the spikes and sinusoids between the different types of fault varies, but the general behavior is the same. All being considered, we decide to use only the third principal component as a representation of the signals, being them used for the remaining calculations.

Applying the cumulants as formulated in Eqs. (11)–(13) for each third principal component signal, a total of features equal to three times the signal length is produced, requiring a dimensionality reduction. Using the multiclass FDR, Eq. (15), a score is assigned to each cumulant and those with the highest score can be interpreted as the ones with the greatest distance between the classes in that dimension. We decided to use only the best lag of each cumulant, reducing the classification problem to a three-dimensional space. The selected features were the lags $\mathbf{c_2}[16184]$, $\mathbf{c_3}[72459]$ and $\mathbf{c_4}[19121]$, where $\mathbf{c_2}$, $\mathbf{c_3}$ and $\mathbf{c_4}$ are the second-, third-, and fourth-order cumulant feature vectors, respectively, for each load/condition combination analysed, as described in section 3.3. With this, we found a considerable dimension reduction from 297003 (99001 for each cumulant) to 3. Note that the cumulants were normalized to the range $[-1, 1]$, as in Eq. (14) before being selected. Figs. 11–13 show the plots of the pairwise resulting feature space.

We can see that the three classes are well separated in this new feature space, indicating that only these three features can be enough for a good distinction between them. It is worth mentioning that, in the case of faults, we found indications that they can also be distinguished between their different types with little or no addition of features. This capability will be further explored in future work.

Finally, the classification was performed by the RBFN. For its construction, we used an error goal (MSE) of 10^{-3} and a spread of $s = 0.25$, the network training was then performed as described in the section 4. For the linear layer, we adopted three output neurons. Therefore, the final architecture of the neural network has two layers with a total of 11 RB neurons in the first and 3 linear neurons in the second. For this configuration, the network achieved a classification rate of 100%, being able to correctly identify the islanding conditions even in the worst scenarios. Table 3 presents the comparison of accuracy between the UVP/OVP, UFP/OFP, and ROCOF IDMs and the proposed method.

It should be remembered that the methods implemented in relay protection cannot distinguish between islanding or fault, so the results presented in Table 3 consider a correct classification whenever the relay trips under islanding or fault conditions. It is worth mentioning that the ROCOF method, one of the most used IDM, as well as the under-frequency relay, were able to correctly identify all cases of islanding, but were not able to identify faults. Finally, it is also pointed out that the classes are unbalanced, with 9 examples of nominal operation, 9 of islanding, and 99 of fault. This occurs because of the way we design this dataset, as described in section 3.3, with eleven types of faults being simulated for each load profile, this class became overrepresented.

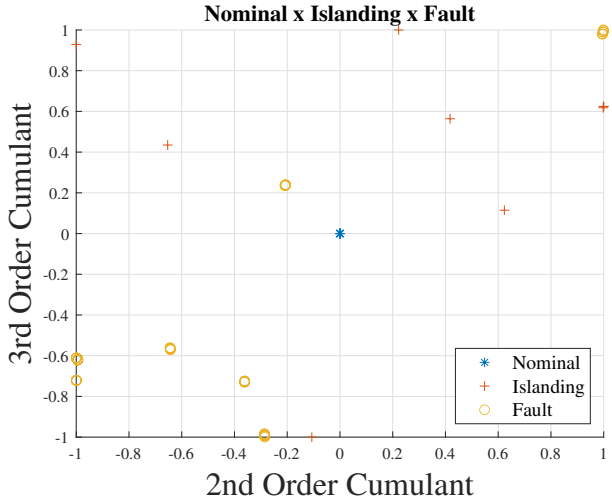

Figure 11: Scatter plot of the three classes considering $\mathbf{c_2}[16184]$ and $\mathbf{c_3}[72459]$.

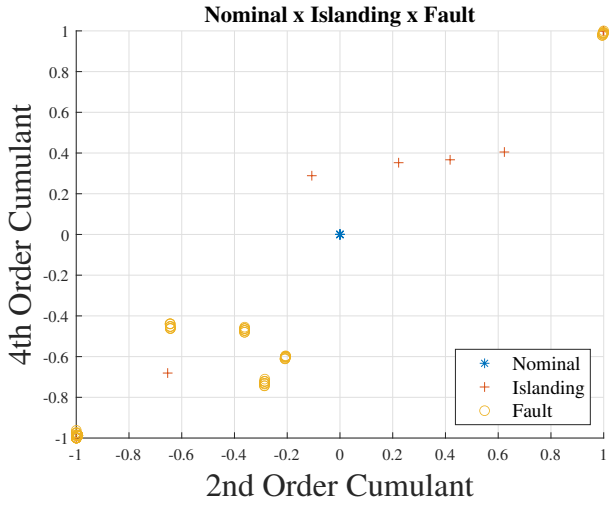

Figure 12: Scatter plot of the three classes considering $\mathbf{c_2}[16184]$ and $\mathbf{c_4}[19121]$.

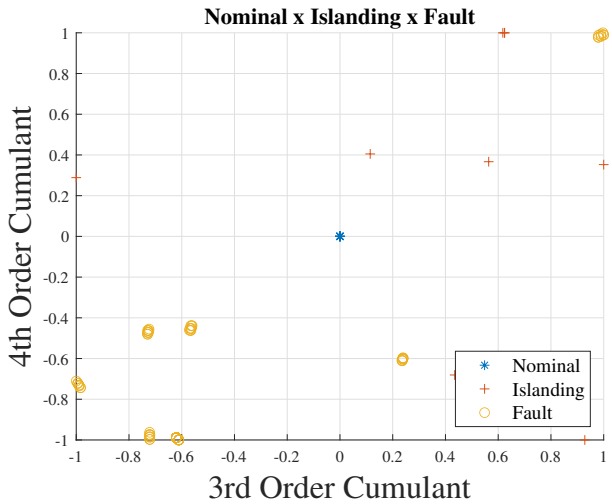

Figure 13: Scatter plot of the three classes considering $\mathbf{c_3}[72459]$ and $\mathbf{c_4}[19121]$.

Table 3: Accuracy of tested passive IDMs

Method	Nominal	Islanding	Fault	Total
Proposed Method	100%	100%	100%	100%
UVP [7]	100%	33.3%	100%	94.87%
OVP [7]	100%	33.3%	54.54%	56.41%
UFP [7]	100%	100%	0%	15.38%
OFP [7]	100%	0%	0%	7.69%
ROCOF [58]	100%	100%	0%	15.38%

5.2 Validation Results

Once designed, the method was applied in the validation set which is composed of the simulation of the three conditions under 100 random power profiles, as described in section 3.3. We extracted the third principal component of the signals using the third column of $\mathbf{R}$, calculate $\mathbf{c_2}[16184]$, $\mathbf{c_3}[72459]$ and $\mathbf{c_4}[19121]$, and applied the normalization. The resulting feature space for this dataset is shown in Figs.14–16.

Table 4 shows the comparison of the tested methods. The proposed method was able to identify 79 of the 100 islanding events, with the other 21 being incorrectly classified as faults. It's a remarkable (and expected) result when we considered that the RBFN was designed using only 9 examples of islanding with unbalanced classes towards the fault. The UVP method was also able to achieve good results, being able to correctly identify 63 islanding events.

Table 4: Accuracy of tested passive IDMs for the validation set

Method	Nominal	Islanding	Fault	Total
Proposed Method	100.00%	79.00%	100.00%	93.00%
UVP [7]	100.00%	63.00%	100.00%	87.67%
OVP [7]	100.00%	22.00%	55.00%	59.00%
UFP [7]	100.00%	100.00%	0.00%	66.67%
OFP [7]	100.00%	0.00%	0.00%	33.33%
ROCOF [58]	100.00%	100.00%	0.00%	66.67%

Finally, in face of the validation results presented in Table 4 and the known unbalance in the design set, we tried to redesign only the RBFN using both sets and performing k-fold cross-validation with 5 folds. Using this approach, the method obtained an average total performance of $99.04 \pm 1.00\%$, with an islanding detection rate of $96.52 \pm 3.27\%$. Since all analyzed cases are within the NDZ allowed by IEEE Std. 1547–2003, we consider this a remarkable detection rate.

5.3 Performance in a Noisy Environment

To evaluate the performance on noisy data, the training and validation datasets were used together and k-fold cross-validation with 5 partitions was performed. As described in Session 3.3, white Gaussian noise, with SNR ranging from 50 to 80 dB, was added to the data. All pre-processing was performed as originally proposed, and only the classifier was remodeled. The results are shown in Table 5.

Table 5: Accuracy of the proposed method in noisy data.

SNR	Accuracy
Without Noise	$99.04 \pm 1.00\%$
50dB	$73.85 \pm 3.19\%$
60dB	$75.77 \pm 6.56\%$
70dB	$76.23 \pm 5.38\%$
80db	$76.26 \pm 3.04\%$

As it can be seen, the method had a performance decrease when applied to noisy data. The main problem observed was the false classification of nominal data as islanding. The fault identification did not have its performance affected. To address this problem, we must carry out a more careful study with these data and redesign the parameters used mainly in the pre-processing stage. We believe that no profound changes in methodology should be made, as indicated by the fault identification performance, which was not affected.

6 CONCLUSIONS

This paper presents a passive method for islanding detection using signal processing tools. It's based on PCA and cumulants to extract relevant information from the three-phase voltage signal. It was tested on a 250kW PV array DG with multiple load

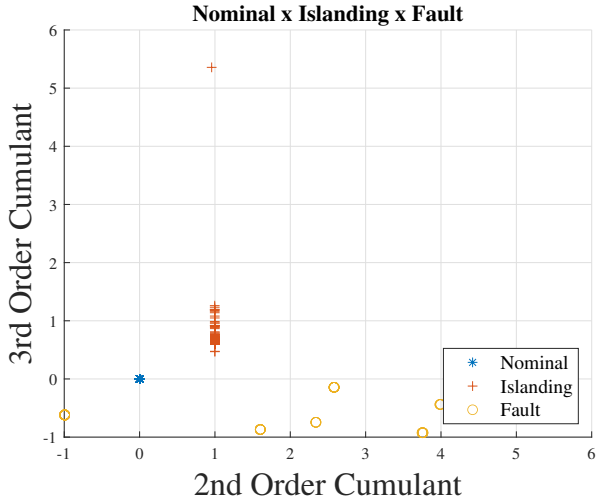

Figure 14: Scatter plot of the validation database considering $\mathbf{c_2}[16184]$ and $\mathbf{c_3}[72459]$.

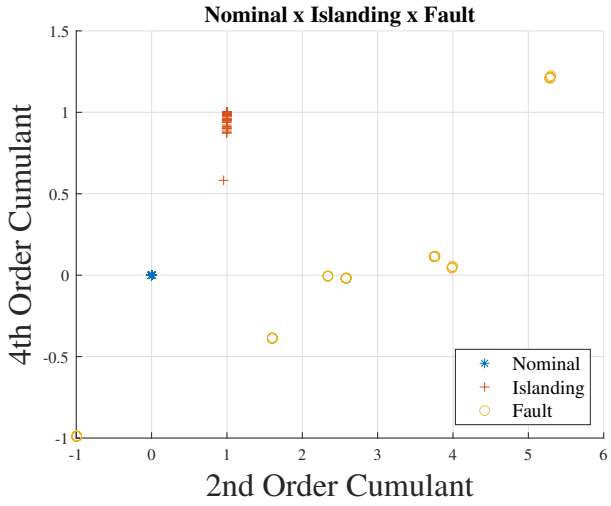

Figure 15: Scatter plot of the validation database considering $\mathbf{c_2}[16184]$ and $\mathbf{c_4}[19121]$.

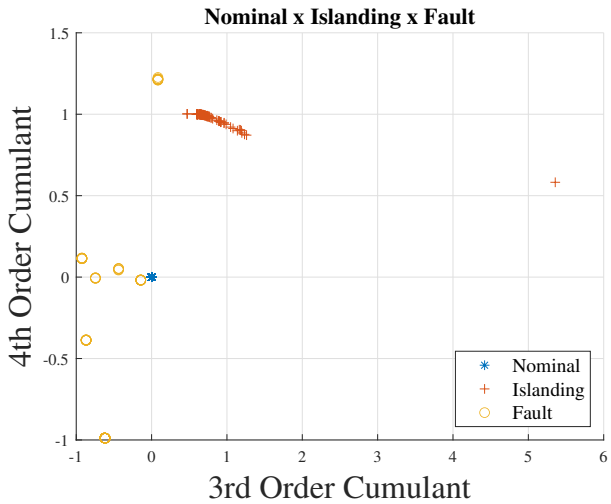

Figure 16: Scatter plot of the validation database considering $\mathbf{c_3}[72459]$ and $\mathbf{c_4}[19121]$.

power requirements against nominal, islanding, and fault operations. It presents an innovative methodology for pre-processing and feature extraction for the ID problem, opening a new way of approaching the subject.

Using the best features from the second-, third-, and fourth-order cumulants calculated from the third principal component, the method was able to perform a classification rate of 99% in a three-dimensional space using RBFN, achieving a negligible NDZ. Although all the processing in this article was performed offline, the method is still valid as a proof of concept and we believe that it will still achieve high detection rates in an online environment. When applied to noisy data, the method obtained a performance loss reaching performances slightly above 73%. It should be noted that all data used is within the ZND allowed by IEEE Std. 1547–2003.

In future works, the aforementioned conversion of the method to an online environment is intended. In addition, we intend to conduct a more accurate study for noisy data and adapt the method to this scenario, in addition to perform a comparison with other passive and signal processing methods in terms of classification rate, response time and computational complexity.

ACKNOWLEDGEMENTS

The authors would like to thank the Coordenação de Aperfeiçoamento de Pessoal de Nível Superior – Brasil (CAPES), the Brazilian National Council for Scientific and Technological Development (CNPq), the National Institute of Science and Technology in Electric Energy (INERGE) and the Minas Gerais State Agency for Research and Development (FAPEMIG) for supporting and financing this study.

REFERENCES

[1] IEC. *Grid integration of large-capacity renewable energy sources and use of large-capacity electrical energy storage : white paper*. IEC, Geneva, 2012.

[2] ANEEL. *Matriz elétrica brasileira*. Agência Nacional de Energia Elétrica – ANEEL, 2022.

[3] ABGD. *Brasil atinge 9 GW de potência instalada em sistemas de geração própria de energia*. Associação Brasileira de Geração Distribuída – ABGD, 2022.

[4] G. A. Quiroga, H. Kagan, J. C. C. Amasifen, C. F. M. Almeida, N. Kagan and E. Vicentini. "Study of the distributed generation impact on distributed networks, focused on quality of power". In *2016 17th International Conference on Harmonics and Quality of Power (ICHQP)*. IEEE, oct 2016.

[5] R. A. Walling and N. W. Miller. "Distributed generation islanding-implications on power system dynamic performance". In *IEEE Power Engineering Society Summer Meeting,*, volume 1, pp. 92–96. IEEE, 2002.

[6] IEEE. "IEEE standard for interconnecting distributed resources with electric power systems". *IEEE Std 1547-2003*, pp. 1–28, 2003.

[7] S. Dutta, P. K. Sadhu, M. J. B. Reddy and D. K. Mohanta. "Shifting of research trends in islanding detection method - a comprehensive survey". *Protection and Control of Modern Power Systems*, vol. 3, no. 1, jan 2018.

[8] M. A. Redfern, O. Usta and G. Fielding. "Protection against loss of utility grid supply for a dispersed storage and generation unit". *IEEE Transactions on Power Delivery*, vol. 8, no. 3, pp. 948–954, jul 1993.

[9] W. Freitas, W. Xu, C. M. Affonso and Z. Huang. "Comparative analysis between ROCOF and vector surge relays for distributed generation applications". *IEEE Transactions on Power Delivery*, vol. 20, no. 2, pp. 1315–1324, apr 2005.

[10] L. A. C. Lopes and H. Sun. "Performance assessment of active frequency drifting islanding detection methods". *IEEE Transactions on Energy Conversion*, vol. 21, no. 1, pp. 171–180, mar 2006.

[11] F. Liu, Y. Kang, Y. Zhang, S. Duan and X. Lin. "Improved SMS islanding detection method for grid-connected converters". *IET Renewable Power Generation*, vol. 4, no. 1, pp. 36, 2010.

[12] M. El-Moubarak, M. Hassan and A. Faza. "Performance of three islanding detection methods for grid-tied multi-inverters". In *2015 IEEE 15th International Conference on Environment and Electrical Engineering (EEEIC)*. IEEE, jun 2015.

[13] M. E. Ropp, M. Begovic and A. Rohatgi. "Prevention of islanding in grid-connected photovoltaic systems". *Progress in Photovoltaics: Research and Applications*, vol. 7, no. 1, pp. 39–59, jan 1999.

[14] M. E. Ropp, M. Begovic and A. Rohatgi. "Analysis and performance assessment of the active frequency drift method of islanding prevention". *IEEE Transactions on Energy Conversion*, vol. 14, no. 3, pp. 810–816, 1999.

[15] B. Wen, D. Boroyevich, R. Burgos, Z. Shen and P. Mattavelli. "Impedance-based analysis of active frequency drift islanding detection for grid-tied inverter system". *IEEE Transactions on Industry Applications*, vol. 52, no. 1, pp. 332–341, jan 2016.

[16] H. H. Zeineldin and S. Conti. "Sandia frequency shift parameter selection for multi-inverter systems to eliminate non-detection zone". *IET Renewable Power Generation*, vol. 5, no. 2, pp. 175, 2011.

[17] X. Wang, W. Freitas, W. Xu and V. Dinavahi. "Impact of DG interface controls on the sandia frequency shift antiislanding method". *IEEE Transactions on Energy Conversion*, vol. 22, no. 3, pp. 792–794, sep 2007.

[18] C. L. Trujillo, D. Velasco, E. Figueres and G. Garcerá. "Analysis of active islanding detection methods for grid-connected microinverters for renewable energy processing". *Applied Energy*, vol. 87, no. 11, pp. 3591–3605, nov 2010.

[19] V. Menon and M. H. Nehrir. "A hybrid islanding detection technique using voltage unbalance and frequency set point". *IEEE Transactions on Power Systems*, vol. 22, no. 1, pp. 442–448, feb 2007.

[20] J. Yin, L. Chang and C. Diduch. "A new hybrid anti-islanding algorithm in grid connected three-phase inverter system". In *37th IEEE Power Electronics Specialists Conference*. IEEE, 2006.

[21] H. Vahedi, R. Noroozian, A. Jalilvand and G. B. Gharehpetian. "Hybrid SFS and q-f islanding detection method for inverter-based DG". In *2010 IEEE International Conference on Power and Energy*. IEEE, nov 2010.

[22] P. Mahat, Z. Chen and B. Bak-Jensen. "A hybrid islanding detection technique using average rate of voltage change and real power shift". *IEEE Transactions on Power Delivery*, vol. 24, no. 2, pp. 764–771, apr 2009.

[23] A. Etxegarai, P. Eguía and I. Zamora. "Analysis of remote islanding detection methods for distributed resources". *Renewable Energy and Power Quality Journal*, pp. 1142–1147, may 2011.

[24] R. A. Walling. "Application of direct transfer trip for prevention of DG islanding". In *2011 IEEE Power and Energy Society General Meeting*. IEEE, jul 2011.

[25] M. Ropp, D. Joshi, R. Reedy, K. Davis, D. Click and A. Shaffer. "New results for power line carrier-based islanding detection and an updated strengths and weaknesses discussion". In *2011 37th IEEE Photovoltaic Specialists Conference*. IEEE, jun 2011.

[26] S. Perlenfein, M. Ropp, J. Neely, S. Gonzalez and L. Rashkin. "Subharmonic power line carrier (PLC) based island detection". In *2015 IEEE Applied Power Electronics Conference and Exposition (APEC)*. IEEE, mar 2015.

[27] Y. Zhu, Q. Yang, J. Wu, D. Zheng and Y. Tian. "A novel islanding detection method of distributed generator based on wavelet transform". In *2008 International Conference on Electrical Machines and Systems*, pp. 2686–2688, 2008.

[28] A. Pigazo, M. Liserre, R. A. Mastromauro, V. M. Moreno and A. Dell'Aquila. "Wavelet-based islanding detection in grid-connected PV systems". *IEEE Transactions on Industrial Electronics*, vol. 56, no. 11, pp. 4445–4455, nov 2009.

[29] M. Hanif, U. D. Dwivedi, M. Basu and K. Gaughan. "Wavelet based islanding detection of dc-ac inverter interfaced dg systems". In *45th International Universities Power Engineering Conference UPEC2010*, pp. 1–5, 2010.

[30] M. Hanif, M. Basu and K. Gaughan. "Development of EN50438 compliant wavelet-based islanding detection technique for three-phase static distributed generation systems". *IET Renewable Power Generation*, vol. 6, no. 4, pp. 289, 2012.

[31] W. G. Morsi, C. P. Diduch and L. Chang. "A new islanding detection approach using wavelet packet transform for wind-based distributed generation". In *The 2nd International Symposium on Power Electronics for Distributed Generation Systems*. IEEE, jun 2010.

[32] S. R. Mohanty, N. Kishor, P. K. Ray and J. P. S. Catalao. "Comparative study of advanced signal processing techniques for islanding detection in a hybrid distributed generation system". *IEEE Transactions on Sustainable Energy*, vol. 6, no. 1, pp. 122–131, jan 2015.

[33] P. K. Ray, S. R. Mohanty and N. Kishor. "Disturbance detection in grid-connected distributed generation system using wavelet and s-transform". *Electric Power Systems Research*, vol. 81, no. 3, pp. 805–819, mar 2011.

[34] A. H. M. Niaki and S. Afsharnia. "A new passive islanding detection method and its performance evaluation for multi-DG systems". *Electric Power Systems Research*, vol. 110, pp. 180–187, may 2014.

[35] S. R. Mohanty, N. Kishor, P. K. Ray and J. P. S. Catalao. "Islanding detection in a distributed generation based hybrid system using intelligent pattern recognition techniques". In *2012 3rd IEEE PES Innovative Smart Grid Technologies Europe (ISGT Europe)*. IEEE, oct 2012.

[36] T. Rabuzin and L. NordstrÃ¶m. "Data-Driven Islanding Detection Using a Principal Subspace of Voltage Angle Differences". *IEEE Transactions on Smart Grid*, vol. 12, no. 5, pp. 4250–4258, 2021.

[37] R. M. Radhakrishnan, A. Sankar and S. Rajan. "Synchrophasor based islanding detection for microgrids using moving window principal component analysis and extended mathematical morphology". *IET Renewable Power Generation*, vol. 14, no. 12, pp. 2089–2099, 2020.

[38] Y. Guo, K. Li, D. M. Laverty and Y. Xue. "Synchrophasor-Based Islanding Detection for Distributed Generation Systems Using Systematic Principal Component Analysis Approaches". *IEEE Transactions on Power Delivery*, vol. 30, no. 6, pp. 2544–2552, 2015.

[39] X. Liu, D. M. Laverty, R. J. Best, K. Li, D. J. Morrow and S. McLoone. "Principal Component Analysis of Wide-Area Phasor Measurements for Islanding Detection–A Geometric View". *IEEE Transactions on Power Delivery*, vol. 30, no. 2, pp. 976–985, 2015.

[40] K. El-Arroudi, G. Joos, I. Kamwa and D. T. McGillis. "Intelligent-based approach to islanding detection in distributed generation". *IEEE Transactions on Power Delivery*, vol. 22, no. 2, pp. 828–835, apr 2007.

[41] Y. Fayyad and A. Osman. "Neuro-wavelet based islanding detection technique". In *2010 IEEE Electrical Power & Energy Conference*. IEEE, aug 2010.

[42] M. S. ElNozahy, E. F. El-Saadany and M. M. A. Salama. "A robust wavelet-ANN based technique for islanding detection". In *2011 IEEE Power and Energy Society General Meeting*. IEEE, jul 2011.

[43] N. W. A. Lidula and A. D. Rajapakse. "Fast and reliable detection of power islands using transient signals". In *2009 International Conference on Industrial and Information Systems (ICIIS)*. IEEE, dec 2009.

[44] S. R. Mohanty, P. K. Ray, N. Kishor and B. K. Panigrahi. "Classification of disturbances in hybrid DG system using modular PNN and SVM". *International Journal of Electrical Power & Energy Systems*, vol. 44, no. 1, pp. 764–777, jan 2013.

[45] M. H. Wang, M.-L. Huang and K.-J. Liou. "Islanding detection method for grid connected photovoltaic systems". *IET Renewable Power Generation*, vol. 9, no. 6, pp. 700–709, aug 2015.

[46] H. T. Do, X. Zhang, N. V. Nguyen, S. Li and T. T.-T. Chu. "Passive islanding detection method using wavelet packet transform in grid connected photovoltaic systems". *IEEE Transactions on Power Electronics*, pp. 1–1, 2015.

[47] E. Rosolowski, A. Burek and L. Jedut. "A new method for islanding detection in distributed generation". *Wroclaw University of Technology: Wrocław, Poland*, 2007.

[48] S. R. Samantaray, K. El-Arroudi, G. Joos and I. Kamwa. "A fuzzy rule-based approach for islanding detection in distributed generation". *IEEE Transactions on Power Delivery*, vol. 25, no. 3, pp. 1427–1433, jul 2010.

[49] H. Shayeghi and B. Sobhani. "Zero NDZ assessment for anti-islanding protection using wavelet analysis and neuro-fuzzy system in inverter based distributed generation". *Energy Conversion and Management*, vol. 79, pp. 616–625, mar 2014.

[50] H. Bitaraf, M. Sheikholeslamzadeh, A. M. Ranjbar and B. Mozafari. "Neuro-fuzzy islanding detection in distributed generation". In *IEEE PES Innovative Smart Grid Technologies*. IEEE, may 2012.

[51] S. D. Kermany, M. Joorabian, S. Deilami and M. A. S. Masoum. "Hybrid islanding detection in microgrid with multiple connection points to smart grids using fuzzy-neural network". *IEEE Transactions on Power Systems*, vol. 32, no. 4, pp. 2640–2651, jul 2017.

[52] M. Heidari, G. Seifossadat and M. Razaz. "Application of decision tree and discrete wavelet transform for an optimized intelligent-based islanding detection method in distributed systems with distributed generations". *Renewable and Sustainable Energy Reviews*, vol. 27, pp. 525–532, nov 2013.

[53] M. Vatani, T. Amraee, A. M. Ranjbar and B. Mozafari. "Relay logic for islanding detection in active distribution systems". *IET Generation, Transmission & Distribution*, vol. 9, no. 12, pp. 1254–1263, sep 2015.

[54] D. S. Broomhead and D. Lowe. "Radial basis functions, multi-variable functional interpolation and adaptive networks". techreport, Royal Signals and Radar Establishment Malvern (United Kingdom), March 1988.

[55] MathWorks. *250-kW Grid-Connected PV Array*. MathWorks, 2022.

[56] J. J. Nedumgatt, K. B. Jayakrishnan, S. Umashankar, D. Vijayakumar and D. P. Kothari. "Perturb and observe MPPT algorithm for solar PV systems-modeling and simulation". In *2011 Annual IEEE India Conference*. IEEE, dec 2011.

[57] G.-C. Hsieh and J. C. Hung. "Phase-locked loop techniques. A survey". *IEEE Transactions on Industrial Electronics*, vol. 43, no. 6, pp. 609–615, dec 1996.

[58] I. V. Banu and M. Istrate. "Islanding prevention scheme for grid-connected photovoltaic systems in Matlab/Simulink". In *2014 49th International Universities Power Engineering Conference (UPEC)*. IEEE, sep 2014.

[59] Z. Ye, A. Kolwalkar, Y. Zhang, P. Du and R. Walling. "Evaluation of anti-islanding schemes based on nondetection zone concept". *IEEE Transactions on Power Electronics*, vol. 19, no. 5, pp. 1171–1176, sep 2004.

[60] H. Abdi and L. J. Williams. "Principal component analysis". *Wiley Interdisciplinary Reviews: Computational Statistics*, vol. 2, no. 4, pp. 433–459, jun 2010.

[61] D. D. Ferreira, C. A. G. Marques, J. M. e de Seixas, A. S. Cerqueira, M. V. Ribeiro and C. A. Duque. "Exploiting higher-order statistics information for power quality monitoring". In *Power Quality*, chapter 17, pp. 345–362. InTech, apr 2011.

[62] S. Theodoridis and K. Koutroumbas. "Pattern recognition and neural networks". In *Machine Learning and Its Applications*, pp. 169–195. Springer Berlin Heidelberg, 2001.